# Poly-crystalline Silicon Thin Film Transistor: a Two-dimensional Threshold Voltage Analysis using Green's Function Approach

**Amit Sehgal*, Tina Mangla**, Mridula Gupta**, and R. S. Gupta****

**Abstract—A two–dimensional treatment of the potential distribution under the depletion approximation is presented for poly–crystalline silicon thin film transistors. Green's function approach is adopted to solve the two–dimensional Poisson's equation. The solution for the potential distribution is derived using Neumann's boundary condition at the silicon–silicon di–oxide interface. The developed model gives insight into device behavior due to the effects of traps and grain–boundaries. Also short–channel effects and drain induced barrier lowering effects are incorporated in the model. The potential distribution and electric field variation with various device parameters is shown. An analysis of threshold voltage is also presented. The results obtained show good agreement with simulated results and numerical modeling based on the finite difference method, thus demonstrating the validity of our model.**

***Index Terms*—Poly–silicon TFT, modeling, grain–boundary effects, short channel effects, drain–induced barrier lowering**

## I. INTRODUCTION

Recently polycrystalline silicon (poly–*Si*) thin–film transistors (TFTs) have emerged as the device of choice for many applications with desirable electrical characteristics. These include, the integrating driver circuits and pixel transistors on the same glass panel, active matrix liquid crystal displays (AMLCDs) in notebook computers and high definition televisions (HDTVs), printer heads, scanners, synchronous random access memories (SRAMs), image sensors, high performance electrically erasable programmable read only memories (EEPROMs), three–dimensional large scale integrated (LSI) circuits and system–on–panel applications [1–5]. Also, a high–resolution active–matrix microencapsulated electrophoretic display (EDP) driven by polycrystalline–silicon thin–film transistors (poly–*Si* TFTs) with integrated drivers have been developed [6]. However, the conventional poly–*Si* TFTs have poor field effect mobility and high leakage current due to the grain–boundaries in the channel region [7–8]. The random distribution of grain sizes and grain–boundary locations lead to unacceptable degradation of device performance for very large scale integrated (VLSI) applications [9]. As the dimensions of poly–*Si* TFTs are reduced to sub–micrometer scale [10], a decrease in the number of grain–boundaries occurs and this leads to many favorable characteristics such as higher mobility, steeper sub–threshold slope, lower threshold voltage and lower leakage current. A successful design of circuits using poly–*Si* TFTs requires a proper understanding of its electrical properties. Several models (physics based, empirical and analytical) have been proposed to predict the characteristics of poly–*Si* TFTs [11–21] but these do not give insight into the device behavior due to the effects

Manuscript received Jul. 3, 2007; revised Nov. 6, 2007.
* Department of Physics and Electronics, Hansraj College, University of Delhi, Delhi – 110007, INDIA
E-mail: amitsehgal112@yahoo.com
** Semiconductor Device Research Laboratory, Department of Electronic Science, University of Delhi South Campus, New Delhi – 110021, INDIA
E-mail: rsgu@bol.net.in

of traps and grain–boundaries. Thus, the need arises to formulate a model that gives insight into the effects of traps and grain–boundaries.

The electrical properties of poly–*Si* films have been interpreted in terms of two distinct models: (i) the segregation theory [22] and (ii) the grain–boundary trapping theory [23], and are used to characterize poly-*Si* TFTs. The upcoming problem in electrostatics is the complication occurring due to the non–linearity of Poisson's equation, and further in the case of short–channel devices, determining the potential distribution becomes a more complex process as Poisson's equation becomes a two–variable problem. This problem has led to the use of the depletion approximation (sub–threshold regime) in our analysis. In order to model the two–dimensional (2–D) characteristics of short–channel poly–*Si* TFTs, Green's function technique is used to determine the exact solution of 2–D Poisson's equation and can be used for any doping profile.

In Section II, Green's function technique with multi–zone solution for 2–D Poisson's equation is described. The zone under consideration is enclosed within a box traced by dashed lines comprising different sub–zones. The solution for 2–D potential distribution in the zone (box) is derived exactly with the given set of boundary conditions and verified by 2–D numerical and simulated results. The derived 2–D potential model incorporates short–channel effects (SCEs) and drain induced barrier lowering (DIBL) effects, and is utilized to demonstrate the electric field, and to evaluate the threshold voltage. Results so obtained are also discussed. Lastly, Section III comprises concluding remarks on the work done.

## II. MODELING and DISCUSSION

### 2.1 Potential Distribution Model

The basic structure of poly–*Si* TFT analogues to silicon–on–insulator metal oxide semiconductor field effect transistor (SOI MOSFET) [24] with single crystal silicon (c–*Si*) film replaced by poly–*Si* thin film (active region) and the gate adjacent to buried oxide is absent. Fig.1 shows the schematic of the ensemble device with break line describing *j* number of grain–boundaries present in the poly–*Si* film. The zone enclosed within the dashed lines is further categorized as different sub–

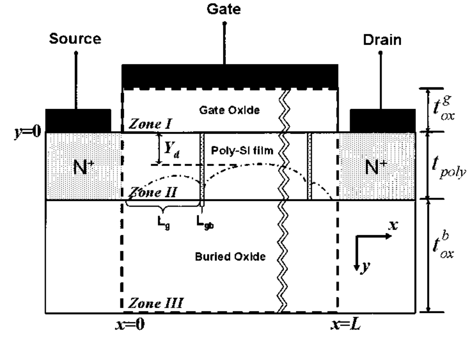


**Fig. 1.** Schematic diagram of poly–crystalline silicon thin film transistor. In Zone II, curve line shows the two dimensional depletion width and $Y_d$ is also defined. Dash lines show the region under consideration for solving Poisson's equation.

zones. Zone I consists of the gate oxide of the device, zone II represents the poly–*Si* film, and the buried oxide lies in zone III of the device. The 2–D Poisson's equation for the above described system is given as:

$$\frac{\partial^2\Phi(x,y)}{\partial x^2}+\frac{\partial^2\Phi(x,y)}{\partial y^2}=-\frac{\rho(x,y)}{\varepsilon_{Si}} \quad (1)$$

where $\Phi(x,y)$ is the 2–D potential distribution, $\varepsilon_{Si}(\varepsilon_{ox})$ is dielectric permittivity of $Si(SiO_2)$ and $\rho(x,y)$ is the 2–D space charge density in the different zones, and is given as

$$\rho(x,y)=\begin{cases}0 & -t_{ox}^{g}\le y\le 0 \quad zone\ I\\ -q\cdot N_{eff}(x) & 0\le y\le \lambda \quad zone\ II\\ 0 & \lambda\le y\le t_{ox}^{b}+t_{poly} \quad zone\ III\end{cases} \quad (2)$$

Also

$$N_{eff}(x)=\begin{cases}N_{gr} & if\ x\ lies\ in\ grain\\ N_{gb} & if\ x\ lies\ in\ grain\ boundary\end{cases}$$ and

$$\lambda=\begin{cases}Y_d & if\ Y_d\le t_{poly}\\ t_{poly} & if\ Y_d>t_{poly}\end{cases}$$

$q$ is the electronic charge, $N_{gr}(N_{gb})$ is the doping concentration in grain (grain–boundary), $Y_d$ is the one–dimensional depletion width and $t_{poly}$ is thickness of the poly–*Si* film.

The effect of trap/defect states using continuous density of states is incorporated in doping

concentrations $N_{gr}$ and $N_{gb}$. The density of defect states used in the analysis is a combination of exponentially decaying band tail states and Gaussian distribution of mid–gap states. It is assumed that the total density of states comprises two tail bands (donor–like valence band and acceptor–like conduction band) and two deep level bands (acceptor–like and donor–like Gaussian distribution) [23].

$$N_{gr} = N_{A1} + Q_{T1}\ , \quad N_{gb} = N_{A2} + Q_{T2}$$

$Q_{T1}$ and $Q_{T2}$ are the trapped carrier density in the grain and grain–boundary region respectively, and can be determined by integrating the density of states ($g(E)$) and probability of occupation of a trap level [25] ($P(E)$) at energy $E$ from valence band ($E_v$) to conduction band ($E_c$) i.e.

$$Q_T = \int_{E_V}^{E_C} g(E)\cdot P(E)\ dE$$

It can be seen from (1) that Poisson's equation reduces to the Laplace equation for zone I and zone III. Also, solving the equation zone–wise reduces the complexity in calculation of equivalent charge density which arises due to the existence of a common boundary between adjacent zones. Using boundary conditions listed in Table I and Green's function solution [26] for each zone as represented in Table II, the 2–D potential distribution for the given Poisson's equation (1) is obtained.

An expression for 2–D potential distribution using Green's theorem and after substitution of Green's function solutions is

$$\begin{aligned}\Phi(x,y) = & \iint_V \frac{\rho(x',y')}{\varepsilon}\cdot G(x,y;x',y')dx'dy' \\ & + \oint_S \frac{\partial\Phi(x',y')}{\partial n'}\cdot G(x,y;x',y')dS \\ & - \oint_S \Phi(x',y')\cdot\frac{\partial G(x,y;x',y')}{\partial n'}dS'\end{aligned} \tag{3}$$

The general form of the modeled potential distribution in each zone is given as:

$$\begin{aligned}\Phi^{I}(x,y) = & \sum_m 2\frac{1-(-1)^m}{m\pi}V_{geff}\frac{\cosh(k_m y)}{\cosh(k_m t_{ox}^g)}\sin(k_m x) \\ & - \sum_m \frac{D_m^g}{\varepsilon_{ox}}\frac{\sinh(k_m(t_{ox}^g + y))}{k_m\cosh(k_m t_{ox}^g)}\sin(k_m x) \\ & + \sum_n \frac{\cos(k_n^I y)}{\sinh(k_n^I L)}\left[P_n^{SI}\sinh(k_n^I(L-x)) + P_n^{DI}\sinh(k_n^I x)\right]\end{aligned} \tag{4}$$

$$\begin{aligned}\Phi^{II}(x,y) = & \iint_V \frac{\rho(x',y')}{\varepsilon}\cdot G(x,y;x',y')dx'dy' + P_0^{SII}\left(1-\frac{x}{L}\right) + P_0^{DII}\left(\frac{x}{L}\right) \\ & + \sum_n \frac{\cos(k_n^{II} y)}{\sinh(k_n^{II} L)}\left[P_n^{SII}\sinh(k_n^{II}(L-x)) + P_n^{DII}\sinh(k_n^{II} x)\right] \\ & + \sum_m \frac{\sin(k_m x)}{\varepsilon_{Si} k_m \sinh(k_m t_{poly})}\left[D_m^g\cosh(k_m(t_{poly}-y)) - D_m^b\cosh(k_m y)\right]\end{aligned} \tag{5}$$

$$\begin{aligned}\Phi^{III}(x,y) = & \sum_m \frac{D_m^b}{\varepsilon_{ox}}\frac{\sinh(k_m(t_{ox}^b + t_{poly} - y))}{k_m\cosh(k_m t_{ox}^b)}\sin(k_m x) \\ & + \sum_n \frac{\cos(k_n^{III}(y - t_{poly}))}{\sinh(k_n^{III} L)}\left[P_n^{SIII}\sinh(k_n^{III}(L-x)) + P_n^{DIII}\sinh(k_n^{III} x)\right]\end{aligned} \tag{6}$$

**Table I.** The List of Boundary Conditions used in the analysis for different zones and Fourier coefficients of the potential/ electric field displacement for different zones.

$$ZoneI \begin{cases} \phi^I(x,-t_{ox}^g) = V_{gs} - V_{fb}^g \\ \phi^I(0,y) = V_{bi} + \dfrac{V_{bi} - (V_{gs} - V_{fb}^g)}{t_{ox}^g}y \\ \phi^I(L,y) = V_{bi} + V_{ds} + \dfrac{V_{bi} + V_{ds} - (V_{gs} - V_{fb}^g)}{t_{ox}^g}y \\ D^g(x,0) = \varepsilon_{ox}E_y^I(x,0) \end{cases} \quad ZoneII \begin{cases} D^g(x,0) = \varepsilon_{Si}E_y^{II}(x,,0) \\ \phi^{II}(0,y) = V_{bi} \\ \phi^{II}(L,y) = V_{bi} + V_{ds} \\ D^g(x,t_{poly}) = \varepsilon_{Si}E_y^{II}(x,t_{poly}) \end{cases}$$

$$ZoneIII \begin{cases} D^b(x,t_{poly}) = \varepsilon_{ox}E_y^{III}(x,t_{poly}) \\ \phi^{III}(0,y) = V_{bi} - \dfrac{V_{bi}}{t_{ox}^b}(y - t_{poly}) \\ \phi^{III}(L,y) = V_{bi} + V_{ds} - \dfrac{V_{bi} + V_{ds}}{t_{ox}^b} \\ \phi^{III}(x,t_{poly} + t_{ox}^b) = 0 \end{cases}$$

Source and drain side

$$P_n^{Si} = \frac{2}{(t_2 - t_1)}\cdot\int_{t_1}^{t_2}\phi^i(0,y)\cdot\cos(k_n^i y)dy \text{ and}$$

$$P_n^{Di} = \frac{2}{(t_2 - t_1)}\cdot\int_{t_1}^{t_2}\phi^i(L,y)\cdot\cos(k_n^i y)dy \text{ for n=0}$$

$$P_n^{Si} = \frac{2}{(t_2 - t_1)}\cdot\int_{t_1}^{t_2}\phi^i(0,y)dy \text{ and } P_n^{Di} = \frac{2}{(t_2 - t_1)}\cdot\int_{t_1}^{t_2}\phi^i(L,y)dy$$

where i=I, II, III and $t_1 = 0,\ t_2 = t_{ox}^g,\ t_{poly},\ t_{ox}^b$ for zone I, II, III respectively Gate oxide and buried oxide side Si-SiO2 interface

$$D_m^g = \frac{2}{L}\cdot\int_0^L D^g(x,0)\cdot\sin(k_m\cdot x)dx \text{ and}$$

$$D_m^b = \frac{2}{L}\cdot\int_0^L D^b(x,t_{poly})\cdot\sin(k_m\cdot x)dx$$

**Table II.** The Green Function Solution for zone I, II, III

Zone I

$$G^{I}(x,y;x',y')=\begin{cases}\dfrac{2}{L}\sum_{m}\sin(k_m x)\sin(k_m x')\dfrac{\cosh(k_m y)\sinh\left(k_m\left(t_{ox}^{g}+y'\right)\right)}{k_m\cosh\left(k_m\left(t_{ox}^{g}\right)\right)} & y'<y\\ \dfrac{2}{L}\sum_{m}\sin(k_m x)\sin(k_m x')\dfrac{\cosh(k_m y')\sinh\left(k_m\left(t_{ox}^{g}+y\right)\right)}{k_m\cosh\left(k_m\left(t_{ox}^{g}\right)\right)} & y<y'\\ \dfrac{2}{t_{ox}^{g}}\sum_{n}\cos(k_n^{I}y)\cos(k_n^{I}y')\dfrac{\sinh(k_n^{I}x)\sinh\left(k_n^{I}(L-x')\right)}{k_n^{I}\sinh(k_n^{I}L)} & x<x'\\ \dfrac{2}{t_{ox}^{g}}\sum_{n}\cos(k_n^{I}y)\cos(k_n^{I}y')\dfrac{\sinh(k_n^{I}x')\sinh\left(k_n^{I}(L-x)\right)}{k_n^{I}\sinh(k_n^{I}L)} & x'<x\end{cases}$$

Zone II c=1, for n=0
c=2, for n≠0

$$G^{II}(x,y;x',y')=\begin{cases}\dfrac{2}{L}\sum_{m}\sin(k_m x)\sin(k_m x')\dfrac{\cosh(k_m y)\cosh\left(k_m\left(t_{poly}-y'\right)\right)}{k_m\sinh\left(k_m\left(t_{poly}\right)\right)} & y'<y\\ \dfrac{2}{L}\sum_{m}\sin(k_m x)\sin(k_m x')\dfrac{\cosh(k_m y')\cosh\left(k_m\left(t_{poly}-y\right)\right)}{k_m\sinh\left(k_m\left(t_{poly}\right)\right)} & y<y'\\ \dfrac{c}{t_{poly}}\sum_{n}\cos(k_n^{II}y)\cos(k_n^{II}y')\dfrac{\sinh(k_n^{II}x)\sinh\left(k_n^{II}(L-x')\right)}{k_n^{II}\sinh(k_n^{II}L)} & x<x'\\ \dfrac{c}{t_{poly}}\sum_{n}\cos(k_n^{II}y)\cos(k_n^{II}y')\dfrac{\sinh(k_n^{II}x')\sinh\left(k_n^{II}(L-x)\right)}{k_n^{II}\sinh(k_n^{II}L)} & x'<x\end{cases}$$

Zone III

$$G^{III}(x,y;x',y')=\begin{cases}\dfrac{2}{L}\sum_{m}\sin(k_m x)\sin(k_m x')\dfrac{\cosh\left(k_m\left(y-t_{poly}\right)\right)\sinh\left(k_m\left(t_{ox}^{b}+t_{poly}-y'\right)\right)}{k_m\cosh\left(k_m\left(t_{ox}^{b}\right)\right)} & y<y'\\ \dfrac{2}{L}\sum_{m}\sin(k_m x)\sin(k_m x')\dfrac{\cosh\left(k_m\left(y'-t_{poly}\right)\right)\sinh\left(k_m\left(t_{ox}^{b}+t_{poly}-y\right)\right)}{k_m\cosh\left(k_m\left(t_{ox}^{g}\right)\right)} & y'<y\\ \dfrac{2}{t_{ox}^{b}}\sum_{n}\cos\left(k_n^{III}\left(y-t_{poly}\right)\right)\cos\left(k_n^{III}\left(y'-t_{poly}\right)\right)\dfrac{\sinh(k_n^{III}x)\sinh\left(k_n^{III}(L-x')\right)}{k_n^{III}\sinh(k_n^{III}L)} & x<x'\\ \dfrac{2}{t_{ox}^{b}}\sum_{n}\cos\left(k_n^{III}\left(y-t_{poly}\right)\right)\cos\left(k_n^{III}\left(y'-t_{poly}\right)\right)\dfrac{\sinh(k_n^{III}x')\sinh\left(k_n^{III}(L-x)\right)}{k_n^{III}\sinh(k_n^{III}L)} & x'<x\end{cases}$$

where $\Phi^{I}(x,y)$, $\Phi^{II}(x,y)$ and $\Phi^{III}(x,y)$ are the potential distributions in zone I, zone II and zone III respectively. $L$ is the effective channel length and $t_{ox}^{g}\left(t_{ox}^{b}\right)$ is the thickness of gate oxide (buried oxide). $V_{bi}$ is the built–in potential of the source(drain)/ body junctions and $V_{ds}$ is drain–source voltage. $V_{geff}=V_{gs}-V_{fb}$ in which $V_{gs}$ is the gate–source voltage and $V_{fb}$ is flat–band voltage. $k_n^{i}$ defines the eigenvalue along $y$ direction of zone $i$ ($i$=I, II, III) ($k_n^{I}=(n-0.5)\cdot\pi/t_{ox}^{g}$, $k_n^{II}=n\cdot\pi/t_{poly}$, $k_n^{III}=(n-0.5)\cdot\pi/t_{ox}^{b}$ for zone I, II, III respectively) and $k_m=m\cdot\pi/L$ is the eigenvalue in all zones along $x$ direction. The Fourier coefficients $P_n^{SI}\left(P_n^{DI}\right)$, $P_n^{SII}\left(P_n^{DII}\right)$, $P_0^{SII}\left(P_0^{DII}\right)$, $P_n^{SIII}\left(P_n^{DIII}\right)$ for the potential distribution at source(drain) end are defined in Table I and that of the electric field displacement ($D_m^{g}\left(D_m^{b}\right)$) at gate oxide(buried oxide) side *Si–SiO₂* interface are unknown as the electric field distributions at the same interfaces are unpredictable (*Neumann's boundary condition*). So, in order to obtain a 2–D solution, $D_m^{g}\left(D_m^{b}\right)$ must be evaluated. These Fourier coefficients can be expressed by equating (4) and (5) at $y=0$, and (5) and (6) at $y=t_{poly}$, and reduced form equations in order to evaluate expressions for $D_m^{g}\left(D_m^{b}\right)$ are given in Appendix.

In poly–*Si* TFTs, the contributing potential due to space charge density reduces to zero for zone I and III as $\rho(x,y)$ is equal to zero, but for zone II (poly–*Si* film) is expressed as

$$\iint_{V}\frac{\rho(x',y')}{\varepsilon}\cdot G(x,y;x',y')dx'dy'=\int_{0}^{x}\left(\frac{-q\cdot N_{eff}(x')}{\varepsilon_{Si}}\cdot\left(\int_{0}^{y}G(x,y,x',y')dy'+\int_{y}^{t_{poly}}G(x,y,x',y')dy'\right)\right)dx'+\int_{x}^{L}\left(\frac{-q\cdot N_{eff}(x')}{\varepsilon_{Si}}\cdot\left(\int_{0}^{y}G(x,y,x',y')dy'+\int_{y}^{t_{poly}}G(x,y,x',y')dy'\right)\right)dx' \quad (7)$$

Hence, the first term in (5) is replaced by (7). In order to demonstrate the validity of our model, the calculated results using (5) in the active device region (poly–*Si* film) are compared with simulated results [27] and numerical model. The numerical modeling is based on finite difference method with the same set of boundary conditions and space charge density distribution.

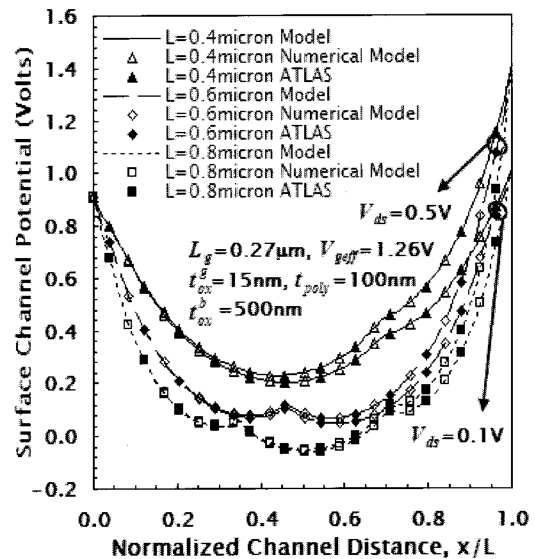


**Fig. 2.** Variation of surface channel potential with normalized channel distance at different channel lengths and drain–source voltage values with doping density $N_{A1}=10^{23}\text{m}^{-3}$ and $N_{A2}=10^{16}\text{m}^{-3}$.

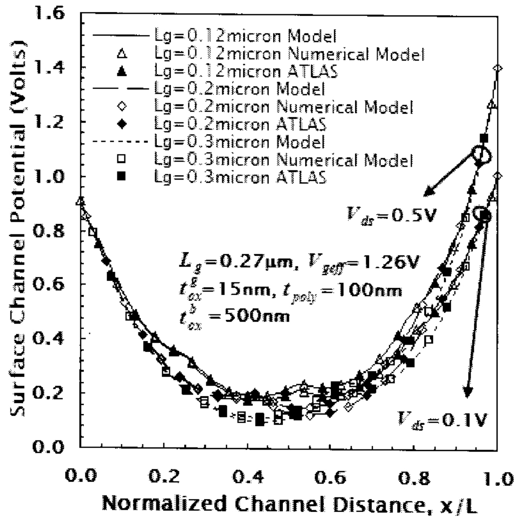


**Fig. 3.** Variation of surface channel potential with normalized channel distance at different grain sizes and drain–source voltage values.

The variation of surface channel potential ($\varphi_c$) with normalized channel distance (*x/L*) is plotted in Fig.2. The figure shows the channel potential at various channel lengths ($L$=0.4μm, 0.6μm, 0.8μm) and drain–source voltage values ($V_{ds}$ = 0.1V, 0.5V) together with numerical results. An excellent matching with simulated results using ATLAS simulator [27] and numerical model shows the validity of our model. It can be seen from the figure that as the channel length is reduced a rise in the value of channel potential occurs, thus depicting the incorporation of SCEs. Also, the comparison of curves at different drain–source voltages shows the existence of the DIBL effect as drain–source voltage increases, which raises the channel potential realized by decrease in energy barrier. The figure also shows the grain–boundary regions demonstrated as potential barriers, acting as trap centers for the flow of carriers. To analyze the effect of grain size, the variation of surface channel potential ($\varphi_c$) with normalized channel distance (*x/L*) at various grain sizes ($L_g$=0.12μm, 0.2μm, 0.3μm) and drain–source voltage values ($V_{ds}$ = 0.1V, 0.5V) is plotted in Fig.3. It is seen that the value of the minimum channel potential rises as the number of barriers increases in the channel. The figure also shows the number of grains available in the channel with formation of potential barriers after each grain end, i.e. at the grain–boundary region.

## 2.2 Horizontal Electric Field at *Si-SiO₂* Interface

The expression for the horizontal electric field, $\xi_c$ at the front end of $Si$–$SiO_2$ interface ($y=0$) is given as

$$\begin{aligned}\xi_c = & \frac{\partial}{\partial x}\left(\iint_V \frac{\rho(x',y')}{\varepsilon}\cdot G(x,y;x',y')dx'dy'\right) + P_0^{SII}\left(-\frac{1}{L}\right) + P_0^{DII}\left(\frac{1}{L}\right) \\ & + \sum_n \frac{k_n^{II}}{\sinh(k_n^{II}L)}\left[-P_n^{SII}\cosh(k_n^{II}(L-x)) + P_n^{DII}\cosh(k_n^{II}x)\right] \\ & + \sum_m \frac{\cos(k_m x)}{\varepsilon_{Si}\sinh(k_m t_{poly})}\left[D_m^g\cosh(k_m(t_{poly})) - D_m^b\right]\end{aligned} \quad (8)$$

The horizontal electric field is formulated to extract the position of minimum surface channel potential ($x_{\min}$) by equating (8) to zero. The extracted minimum surface potential position is placed in (5) to obtain the value of the minimum surface channel potential. Further, in the electric field analysis of poly–*Si* TFT, the first term in (8) is replaced by the derivative of expression (7) and can be expressed as

$$\begin{aligned}\frac{\partial}{\partial x}\left(\iint_V \frac{\rho(x',y')}{\varepsilon}\cdot G(x,y;x',y')dx'dy'\right) = & \int_0^x\left(\frac{-q\cdot N_{eff}(x')}{\varepsilon_{Si}}\cdot\left(\int_0^y\frac{\partial G(x,y,x',y')}{\partial x}dy' + \int_y^{t_{poly}}\frac{\partial G(x,y,x',y')}{\partial x}dy'\right)\right)dx' \\ & + \int_x^L\left(\frac{-q\cdot N_{eff}(x')}{\varepsilon_{Si}}\cdot\left(\int_0^y\frac{\partial G(x,y,x',y')}{\partial x}dy' + \int_y^{t_{poly}}\frac{\partial G(x,y,x',y')}{\partial x}dy'\right)\right)dx'\end{aligned} \quad (9)$$

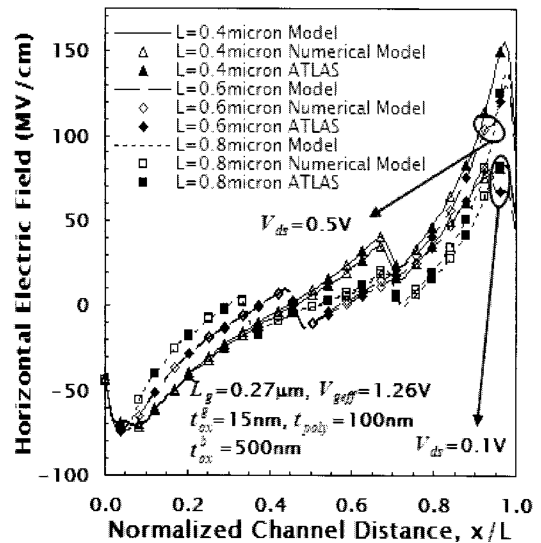


**Fig. 4.** Variation of horizontal surface electric field with normalized channel distance at different channel lengths and drain–source voltage values.

The electric field distribution and potential distribution gives insight into device physics for the proper understanding of device behavior and contains no fitting parameters. The 2–D analysis shows the effects of various device parameters such as channel length, drain bias on the device characteristics.

Fig.4 shows the horizontal electric field ( $\xi_c$ ) distribution at the surface (*y=0*) with normalized channel distance (*x/L*) at various channel lengths (*L*=0.4μm, 0.6μm, 0.8μm) and drain–source voltage values ( $V_{ds}$ = 0.1V, 0.5V) together with simulated results [27] and numerical results. This figure shows an abrupt change in the value of the horizontal electric field at the grain–boundaries close to the drain end. This occurs due to the formation of a potential barrier at the grain–boundary that was suppressed by the drain bias (Fig.2). This figure also demonstrates the existence of SCEs incorporated in device modeling and DIBL effect which can be viewed as the rise in its value near drain end. Horizontal electric field variation with normalized channel distance at various grain sizes ( $L_g$ =0.12μm, 0.2μm, 0.3μm) and drain–source voltage values ( $V_{ds}$ = 0.1V, 0.5V) is shown in Fig.5. The grain–boundary region can be seen in the figure as a sudden transition in the value of electric field, (indicating the number of grains) and shows the formation of potential barrier in the defect region.

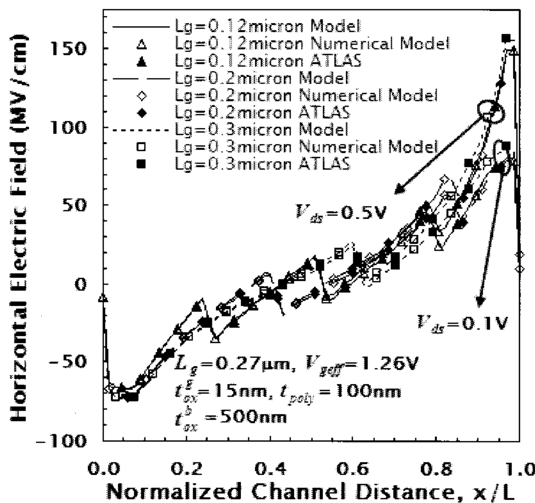


**Fig. 5.** Variation of horizontal surface electric field with normalized channel distance at different grain sizes and drain–source voltage values.

## 2.3 Threshold Voltage

The threshold voltage ( $V_{th}$ ) of the device is one of the most important parameter for circuit, device and process characterization. By modeling aspect, it is referred to as that particular gate voltage at which the minimum surface channel potential is equal to twice the Fermi potential value ( $\phi_{finv}$ ), i.e. the condition for onset of inversion regime.

In our case, while equating the surface horizontal electric field to zero there exist several minima positions ( $x_{\min}$ ). This is due to the barriers in the channel, which causes a sudden change in the electric field value and hence, a point of minima arises. In order to extract the

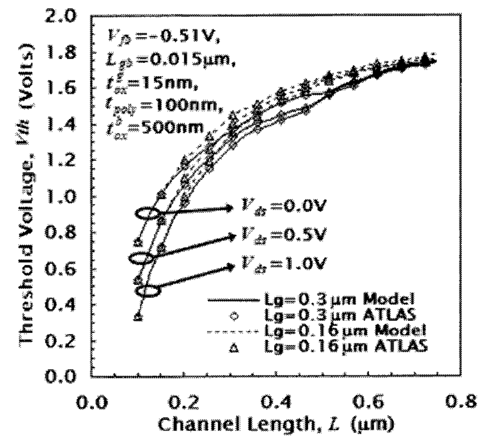


**Fig. 6a.** Variation of threshold voltage with channel length at different grain sizes and drain–source voltage values with doping density $N_{A1}$=$10^{23}$m$^{-3}$ and $N_{A2}$=$10^{16}$m$^{-3}$.

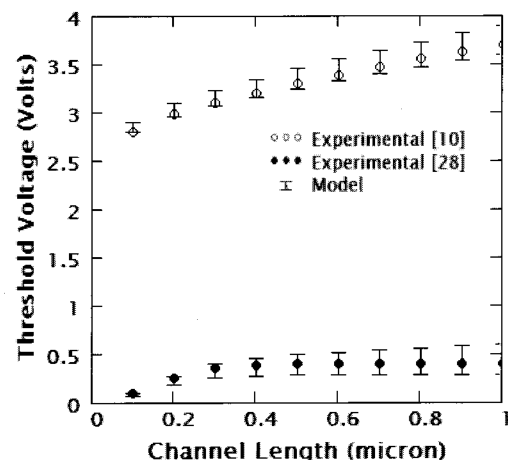


**Fig. 6b.** Variation of threshold voltage with channel length together with experimental results.

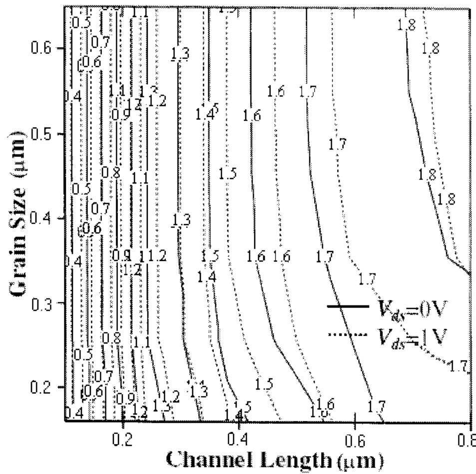


**Fig. 7.** Contour plot of threshold voltage variation with channel length, grain size at different drain voltages.

$V_{th}$ of the device, the surface channel potential at each minima has to be evaluated separately and equated iteratively to $\phi_{finv}$. Thus, the maximum of all threshold voltage values calculated at various minima positions is referred to as the $V_{th}$ of the device.

Threshold voltage, a key parameter required for switching applications, is plotted with channel length at different drain–source voltage values and grain sizes in Fig.6a. The values match remarkably with simulated results [27]. The figure shows roll–off in the value of threshold voltage as we switch towards small dimensions which is in agreement device physics as less value of gate–source voltage is required to deplete the reduced area. The drain bias also contributes to scaling down the threshold voltage value as lateral field induced depletion reduces region of concern required to be depleted. From the figure, for fixed dimensions of grain/grain–boundary, the number of grain–boundaries incorporated in the channel length can be determined. The impact of change in the number of grain–boundaries existing in a particular channel length can also be seen from the figure. The figure shows a rise in the threshold voltage with increase in channel length. For fixed grain dimensions, as channel length increases a larger number of grain–boundaries are incorporated in the channel, thus increasing grain–boundary effects. Also, as the grain dimension switches from 0.16μm to 0.3μm the threshold voltage of the device decreases. This is due to the fact that a lesser number of grain–boundaries are incorporated in the channel, thus lowering the grain–boundary effects. To show the experimental evaluation of our modeled results, Fig. 6b is drawn for the threshold voltage of the device. In the figure, the threshold range is presented which refers to the threshold voltage values at different grain–boundary positions, as the probability of finding the grain–boundary is in–determinant on experimental basis. The results produced i.e. threshold voltage range is in agreement with experimental results [28] thus, justifying our analysis.

Fig. 7 shows the contour plot of threshold voltage for different channel lengths and grain sizes at drain voltages, $V_{ds}$ =0V and 1V. The contour shows that at small channel lengths, the contour lines are near–by/close to each other over a span of various grain sizes. This happens as the device geometry itself reduces to a single grain–boundary value problem when the grain size exceeds the channel length. Thus, the contribution to the device threshold roll–off is only due to the reduction in channel length i.e. SCE that enhances the overall device potential due to reduced area to be depleted. Whereas, when the channel length exceeds the grain size i.e. towards the increasing value of channel length, the role of grain–boundary effect is more prominent, and can be visualized by widening of spacing between different contour lines. The drain voltage when switches from $V_{ds}$=0V to $V_{ds}$=1V, shows a decay in threshold voltage value due to up–raiser of minimum channel potential and in–turn meeting the requirement of $\Phi(x_{\min},0) = \varphi_{finv}$ at earlier gate voltages.

The variation of the minimum surface channel potential position ($x_{min}$) with channel length at various gate–source voltage values and grain sizes is plotted in Fig.8 and its inset. The increase in $x_{min}$ is due to the shifted grain–boundary and increase in the channel length. A sudden transition seen in the curves is due to the transition of device from a single grain–boundary problem to the two grain–boundary problem. As we switch from the two grain–boundary to the three grain–boundary problem and so on, not much of transition is seen in the value of the minimum surface potential position with respect to channel length. This is due to the reason that as more grain–boundaries lie in the channel, their independent effects are suppressed by their mutual effect. Minimum surface channel potential

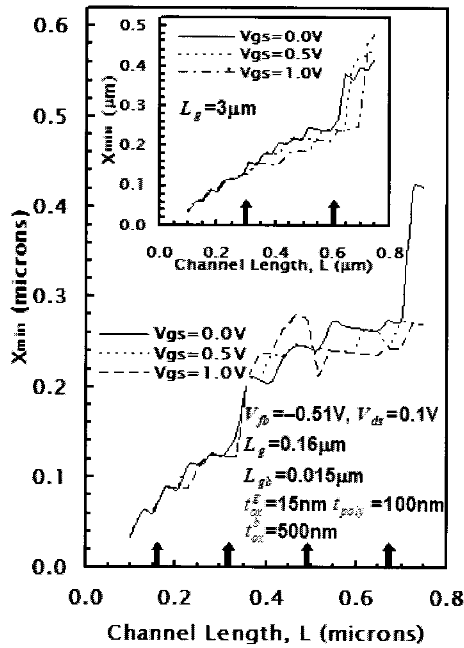


**Fig. 8.** Variation of minimum surface channel potential position, $x_{min}$ with channel length at grain size of 0.16μm for different gate–source voltage values. *Inset* Variation of minimum surface channel potential position, $x_{min}$ with channel length at grain size of 0.3μm for different gate–source voltage values. Arrow heads on channel length axis show the location of grain–boundaries.

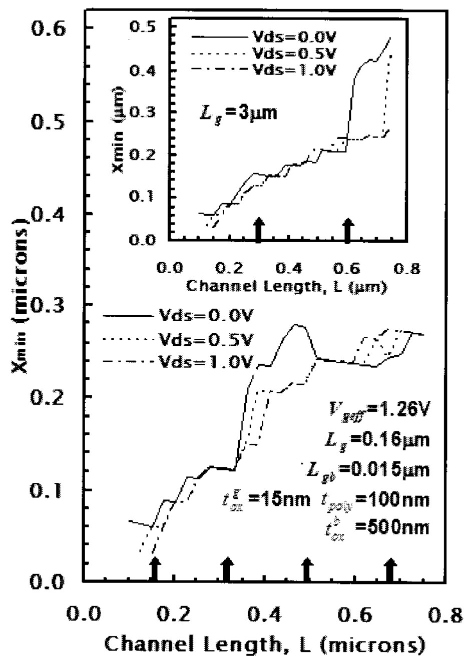


**Fig. 9.** Variation of minimum surface channel potential position, $x_{min}$ with channel length at grain size of 0.16μm for different drain–source voltage values. *Inset* Variation of minimum surface channel potential position, $x_{min}$ with channel length at grain size of 0.3μm for different drain–source voltage values. Arrow heads on channel length axis show the location of grain–boundaries.

position ( $x_{\min}$ ) variation with channel length at different drain–source voltage values and grain sizes can be seen in Fig.9 and its inset. The figure shows that the minimum surface channel potential position shifts towards the source end with the increase in drain bias (DIBL effect). Also a sudden transition in the value of $x_{min}$ is seen whenever there is an increase in the number of grain–boundaries in the channel. On comparison of Fig.9 with its inset, it is seen that for grain size of large dimensions, $x_{min}$ lies near to the drain end. This can be explained as the grain–boundary effect on the channel is suppressed by drain bias.

## III. CONCLUSION

A 2-D model under the depletion approximation is presented for a poly–crystalline silicon thin film transistor. Green's function approach is found to be a promising approach to solve the 2-D Poisson's equation for any arbitrary doping profile. The developed model gives insight into device behavior due to the effects of traps and grain–boundaries. The figures demonstrate the effect of the number of grain–boundaries present in the channel. SCEs and DIBL effects can also be seen from the figures, and as the device dimensions are reduced, these effects contribute in the minimizing of potential barrier generated due to traps at the grain–boundary. The drain bias also affects the channel potential as it overcomes the barriers found close to the drain end. The results obtained show good agreement with simulated results and numerical modeling results based on the finite difference method for the same set of boundary conditions and space charge density distribution.

## ACKNOWLEDGMENT

The authors are thankful to University Grants Commission (UGC), India and Defence Research and Development Organization (DRDO), Ministry of Defence, India for providing financially supporting this research work.

## APPENDIX

(2A) and (3A) are evaluated by (7) at $y$=0 and

$y = t_{poly}$.

$$\alpha_1(m) = \frac{2L}{m\pi}\frac{\left[1-(-1)^m\right]V_{geff}}{2\cosh\left(k_m t_{ox}^g\right)} + \sum_n \left(P_n^{SI} + (-1)^{m+1} P_n^{SI}\right)\frac{k_m}{k_n^{I^2} + k_m^2} \quad (1A)$$

$$\alpha_2(m) = \int_0^L \left( \int_0^{L}\int_0^{t_{poly}} \frac{\rho(x',y')}{\varepsilon_{Si}} G(x,y;x',y')dy'dx' \Big|_{y=0} \right) \sin(k_m x)dx + P_0^{SII}\left(\frac{1-(-1)^m}{k_m}\right) + P_0^{DII}\frac{(-1)^{m+1}}{k_m} + \sum_n \left(P_n^{SII} + (-1)^{m+1} P_n^{DII}\right)\frac{k_m}{k_n^{II^2} + k_m^2} \quad (2A)$$

$$\beta_1(m) = \int_0^L \left( \int_0^{L}\int_0^{t_{poly}} \frac{\rho(x',y')}{\varepsilon_{Si}} G(x,y;x',y')dy'dx' \Big|_{y=t_{poly}} \right) \sin(k_m x)dx + P_0^{SII}\left(\frac{1-(-1)^m}{k_m}\right) + P_0^{DII}\frac{(-1)^{m+1}}{k_m} + \sum_n (-1)^n \left(P_n^{SII} + (-1)^{m+1} P_n^{DII}\right)\frac{k_m}{k_n^{II^2} + k_m^2} \quad (3A)$$

$$\beta_2(m) = \sum_n \left(P_n^{SIII} + (-1)^{m+1} P_n^{DIII}\right)\frac{k_m}{k_n^{III^2} + k_m^2} \quad (4A)$$

$$\gamma_1 = \frac{1}{2m\pi}\left(\frac{\tanh\left(k_m t_{ox}^g\right)}{\varepsilon_{ox}} + \frac{1}{\varepsilon_{Si}\tanh\left(k_m t_{poly}\right)}\right) \quad (5A)$$

$$\gamma_2 = \frac{1}{2m\pi\varepsilon_{Si}\sinh\left(k_m t_{poly}\right)} \quad (6A)$$

$$\gamma_3 = \frac{1}{2m\pi}\left(\frac{\tanh\left(k_m t_{ox}^b\right)}{\varepsilon_{ox}} + \frac{1}{\varepsilon_{Si}\tanh\left(k_m t_{poly}\right)}\right) \quad (7A)$$

$$D_m^g = \frac{(\alpha_1(m) - \alpha_2(m))\gamma_3 - (\beta_2(m) - \beta_1(m))\gamma_2}{\gamma_1\gamma_3 - \gamma_2^2} \quad (8A)$$

$$D_m^b = \frac{(\alpha_1(m) - \alpha_2(m))\gamma_2 - (\beta_2(m) - \beta_1(m))\gamma_1}{\gamma_1\gamma_3 - \gamma_2^2} \quad (9A)$$

## REFERENCES


[1] S. Zhang, C. Zhu, J. K. O. Sin, J. N. Li and P. K. T. Mok, "Ultra-thin elevated channel poly-Si TFT technology for fully-integrated AMLCD system on glass," *IEEE Trans. Electron Devices*, vol. 47, pp. 569-574, 2000.

[2] Z. Meng, M. Wang and M. Wong, "High performance low temperature metal induced unilaterally crystallized polycrystalline silicon thin film transistor for system-on-panel applications," *IEEE Trans. Electron Devices*, vol. 47, pp. 404-409, 2000.

[3] T. Yamanaka, "Advanced TFT SRAM cell technology using a phase shift lithography," *IEEE Trans. Electron Devices*, vol. 42, pp. 1305-1313, 1995.

[4] T. Kaneko, "400-dpi integrated contact type linear image sensors with Poly-Si TFTs analog read out circuits and dynamic shift registers," *IEEE Trans. Electron Devices*, vol. 38, pp.1086-1093, 1991.

[5] M. Cao, T. Zhao, K. Saraswat, and J. Plummer, "A simple EEPROM cell using twin polysilicon thin-film transistors," *IEEE Electron Device Lett.*, vol. 15, pp. 304, 1994.

[6] S. Inoue, H. Kawai, S. Kanbe, T. Saeki and T. Shimoda, "High-resolution microencapsulated electrophoretic display (EDP) driven by poly-Si TFT with four-level grayscale," *IEEE Trans. Electron Devices*, vol. 49, pp. 1532-1539, 2002.

[7] K.R. Olasupo and M.K. Hatalis, "Leakage current mechanism in sub-micron poly-silicon thin-film transistors," *IEEE Trans Electron Devices*, vol. 43, pp. 1218-1223, 1996.

[8] G.A. Bhat, H.S. Kwok and M. Wong, "Behavior of the drain leakage current in metal induced laterally crystallized thin-film transistors," *Solid-State Electron.*, vol. 44, pp. 1321-1324, 2000.

[9] T. Noguchi, "Appearance of single-crystal properties in fine-patterned Si thin-film transistors (TFTs) by solid phase crystallization (SPC)," *Jpn. J. Appl. Phys.*, vol. 32, pp.1584-1587, 1993.

[10] N. Yamauchi, J.J. Hajjar and R. Raif, "Poly-silicon thin-film transistors with channel length and width comparable to or smaller than the grain size of the thin-film," *IEEE Trans. Electron Devices*, vol. 38, pp. 55-59, 1991.

[11] S. Chopra and R.S. Gupta, "An analytical model for current voltage characteristics of short geometry poly Si thin film transistor," *Semiconductor Science and Technology,* vol.15, pp. 1065, 2000.

[12] T. Serikawa, S. Shirai, A. Okamoto, S. Suyama, "A model of current-voltage characteristics in polycrystalline silicon thin film transistor," *IEEE Trans. Electron. Devices*, vol. 34, pp. 321-324, 1987.

[13] P. Lin, J. Guo, and C. Wu, "A quasi two

dimensional analytical model for the turn on characteristics of polysilicon thin film transistors," *IEEE Trans. Electron Devices*, vol. 37, pp. 2463, 1990.

[14] S. Chopra and R.S. Gupta, "An analytical model for turn on characteristics of short channel polycrystalline silicon thin film transistor for circuit simulation," *Microelectronic Eng.*, vol. 54, pp. 263, 2000.

[15] G. Fortunato and P. Migliorato, "Model for the above threshold characteristics and threshold voltage in poly crystalline silicon transistors," *J. Appl. Phys.*, vol. 68, pp. 2463, 1990.

[16] S. Bindra, S. Haldar and R.S. Gupta, "Gate capacitance characteristics of a poly-Si thin film transistor," *Solid-State Electron.*, vol. 48, pp. 675, 2004.

[17] K. Ono, T. Aoyama, N. Konishi, K. Miyata, "Analysis of current – voltage characteristics of low temperature processed polysilicon thin film transistors," *IEEE Trans. Electron Devices*, vol. 39, pp. 792 – 801, 1992.

[18] S. Bindra, S. Haldar, and R.S. Gupta, "Charge sheet model of a polysilicon thin film transistor," *Microelectronic Eng.*, vol. 60, pp. 381, 2002.

[19] H.N. Chern, C.L. Lee, T.F. Lei, "An analytical model for the above threshold characteristics of polysilicon thin film transistors," *IEEE Trans. Electron. Devices*, vol. 42, pp. 1240 – 1246, 1995.

[20] G. Yang, S. Hur, C. Kim, and C. Han, "A physical based analytical turn on model of polysilicon thin film transistors for circuit simulation," in *IEDM Tech. Dig.*, pp. 953, 1995.

[21] S. Chopra and R.S. Gupta, "Modeling of short geometry polycrystalline silicon thin film transistor," *IEEE Trans. Electron. Devices*, vol. 47, pp. 2444, 2000.

[22] J.Y.W. Seto, The electrical properties of polycrystalline silicon films," *J. Appl. Phys.*, vol. 46, pp. 5247-5254, 1975.

[23] G. Baccarani, B. Ricco and G. Spadini, "Transport properties of polycrystalline silicon films," *J. Appl. Phys.*, vol. 49, pp. 5565-5570, 1978.

[24] J.Y. Guo and C.Y. Wu, "A new 2-D analytic threshold voltage model for fully-depleted short-channel SOI MOSFETs," *IEEE Trans. Electron Devices*, vol. 40, pp. 1653-1661, 1993.

[25] S. M. Sze, *Physics of Semiconductor Devices*, John Wiley & Sons, 1981.

[26] J. D. Jackson, *Classical Electrodynamics*, John Wiley & Sons, Inc. 1975.

[27] Atlas User Manual Device Simulator, Silvaco International 2000.

[28] S. Jagar, C. F. Cheng, S. Zhang, H. Wang, M. C. Poon, C. W. Kok and M. Chan, "A SPICE model for thin-film transistors fabricated on grain-enhanced polysilicon film," vol. 50, pp. 1103-8, 2003.

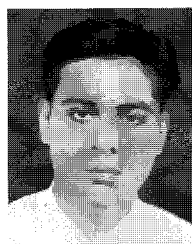

**Amit Sehgal** was born in Delhi, India on December 01, 1979. He received the B.Sc. (Honors) and M.Sc. degrees in electronics from University of Delhi, Delhi, India in 2000 and 2002 respectively. He got Ph. D. degree in Microelectronics at the University of Delhi, Delhi, India in 2007.

He joined Hansraj College, University of Delhi, Delhi, India in year 2005 as lecturer. He joined Semiconductor Device Research Laboratory Department of Electronic Science, University of Delhi South Campus in year 2002. He is listed in 9th edition of Marquis Who's Who in Science and Engineering, premier edition of Marquis Who's Who in Asia and 25th Anniversary Edition of Who's Who in the World. His research interests are in the modeling, simulation and characterization of silicon based devices especially poly-crystalline TFT, gate engineered structures and MOSFETs with quantization effects. He has 26 publications in international and national journals and conferences.

**Tina Mangla** was born in Delhi, India on September 06, 1980. She received the B.Sc.(special) degree in electronics from Gujarat University, Gujarat, India in 2000 and M.Sc. degree in electronics from University of Delhi, Delhi, India in 2002. She got Ph. D. degree in Microelectronics at the University of Delhi, Delhi, India in 2007.
She joined Semiconductor Devices Research Laboratory, Department of Electronic Science, University of Delhi South Campus in 2002. She is listed in 25th Anniversary Edition of Who's Who in the World. Her research interests are in the modeling, simulation and characterization of silicon based devices especially MOSFETs with quantization effects, gate engineered structures and poly-crystalline TFT. She has 26 publications in international and national journals and conferences.

**Mridula Gupta** received the B.Sc. degree in Physics, M.Sc. degree in Electronics, M.Tech. degree in Microwave Electronics, and Ph.D. degree in Optoelectronics from the University of Delhi, Delhi, India, in 1984, 1986, 1988, and 1998, respectively.
In 1989, she joined the Department of Electronic Science, University of Delhi, as a lecturer. She is currently a reader with the University of Delhi. She has authored or coauthored approximately 151 publications in international and national journals and conferences. She contributed the chapter entitled "MOSFET Modeling" in the *Encyclopedia on RF and Microwave Engineering* (New York: Wiley, 2005). Her current research interests include modeling and simulation of MOSFETs, MESFETs, and HEMTs for microwave-frequency applications.
Dr. Gupta is a Fellow of the Institution of Electronics and Telecommunication Engineers, (India), Member IEEE and life member of Semiconductor Society of India. She was Secretary of the 2004 Asia-Pacific Microwave Conference, New Delhi, India, held in December 2004.

**R. S. Gupta** received the B.Sc. and M.Sc. degree from Agra University, India, in 1963 and 1966, respectively, and the Ph.D. degree in electronic engineering form the Institute of Technology, Banaras Hindu University, India in 1970.
In 1971, he joined Ramjas College, University of Delhi, Delhi, India. In 1987, he joined the Department of Electronic Science, University of Delhi, where he is currently a Professor. He heads several major research projects sponsored by the Ministry of Defence, Department of Science and Technology, Council of Science, and Industrial Research and University Grants Commission. In 1988, he was a visitor with the University of Sheffield, Sheffield, UK, under the ALIS Link exchange program and also visited several U.S. and Spanish Universities in 1995 and 1999, respectively. He has authored or coauthored over 392 papers in various international and national journals and conferences. He contributed the chapter entitled "MOSFET Modeling" in the *Encyclopedia on RF and Microwave Engineering* (New York: Wiley, 2005). He has supervised 34 Ph.D. students and 2 students who are currently working toward their Ph.D. degrees. His current interests and activities cover modeling of SOI sub-micrometer MOSFETs and LDD MOSFETs, modeling and design of HEMTs, hot-carrier effects in MOSFETs, and modeling of GaAs MESFETs for high performance microwave and millimeter-wave circuits and Quantum effect devices. He has listed in *Who's Who in the World.* He was a Visitor at the University of Sheffield, Sheffield, U.K., in 1988, under the ALIS Link exchange program and has also visited several U.S. universities in 1995. He has also visited Czech Republic in August 2003, Korea in November 2003, RPI Troy, NY in August 2004, and China in December 2005.
Dr. Gupta was an executive member of the IEEE-Electron Devices (ED)/Microwave Theory and Techniques (MTT) Chapter India Council. His name also appeared in the Golden list of IEEE Transactions on Electron Devices in December 1998, 2002, and 2004. He is a fellow of the Institution of Electronics and telecommunication Engineers (India), a Life member of the Indian Chapter of the International Centre for Theoretical Physics (ICTP), and a Life Member of the

Semiconductor Society of India. He was the secretary of ISRAMT'93 and the 1996 Asia-Pacific Microwave Conference (APMC'96) and the Chairman of the Technical Programme Committee of APMC'96. He edited the proceedings of both of these international conferences. He was chairman of APMC'2004, held in New Delhi, India in December 2004. He was listed in *Who's Who in the World.* He is IEEE-ED Delhi chapter Chairman.